2126 *J. Med. Chem.* **2010,** *53,* 2126–2135
DOI: 10.1021/jm9016416

Journal of
Medicinal
Chemistry
Article

Enhancement of Hydrophobic Interactions and Hydrogen Bond Strength by Cooperativity: Synthesis, Modeling, and Molecular Dynamics Simulations of a Congeneric Series of Thrombin Inhibitors

Laveena Muley,[†] Bernhard Baum,[‡] Michael Smolinski,[†] Marek Freindorf,[§] Andreas Heine,[†] Gerhard Klebe,*[,‡] and David G. Hangauer*[,†]

[†]*Department of Chemistry, University at Buffalo, The State University of New York, Buffalo, New York 14260,*
[‡]*Department of Pharmaceutical Chemistry, Philipps University Marburg, Marbacher Weg 6, 35032 Marburg, Germany, and*
[§]*The Center for Computational Research, University at Buffalo, The State University of New York, Buffalo, New York 14260*

Received November 5, 2009

Accurately predicting the binding affinity of ligands to their receptors by computational methods is one of the major challenges in structure-based drug design. One of the potentially significant errors in these predictions is the common assumption that the ligand binding affinity contributions of noncovalent interactions are additive. Herein we present data obtained from two separate series of thrombin inhibitors containing hydrophobic side chains of increasing size that bind in the S3 pocket and with, or without, an adjacent amine that engages in a hydrogen bond with Gly 216. The first series of inhibitors has a *m*-chlorobenzyl moiety binding in the S1 pocket, and the second has a benzamidine moiety. When the adjacent hydrogen bond is present, the enhanced binding affinity per Å^2 of hydrophobic contact surface in the S3 pocket improves by 75% and 59%, respectively, over the inhibitors lacking this hydrogen bond. This improvement of the binding affinity per Å^2 demonstrates cooperativity between the hydrophobic interaction and the hydrogen bond.

Introduction

Molecular recognition in an aqueous biological system occurs through a collection of reversible and individually weak, binding interactions between the interacting species. As such, it is one of the most important processes in drug discovery. There have been substantial advances in the determination of the structures of proteins and their complexes by X-ray crystallography and NMR[a] spectroscopy.[1] However the ability to quantitatively, or even semiquantitatively, predict the binding affinity of ligands to these structures using computational methods is still a major challenge. In a recent analysis by Warren et al,[2] 10 docking programs and 37 scoring functions were evaluated and it was concluded that the scoring functions are in need of significant improvements for predicting binding affinity. This task is particularly challenging because the observed binding affinity not only is due to the collective weak noncovalent interactions but also includes the ability of the ligand to access the binding site, the desolvation free energy of the ligand, and the protein binding cavity as well as entropy and enthalpy changes in the ligand, protein host, and water.[3−5] Also, scoring functions typically make the assumption that the binding affinity contributed by each of the individual interactions to the total binding affinity is additive and does not depend upon the surrounding interactions.[6] This assumption does not account for one of the confounding properties of noncovalent interactions, namely, that of cooperativity.[7] Cooperativity, as described by Williams,[8] is a phenomenon whereby multiple ligand−host binding interactions can give a ligand with a binding affinity greater than (positive cooperativity) or less than (negative cooperativity) the sum of the individual interactions. For example, a recent paper by Lafleur et al described positive cooperativity between van der Waals interactions and a hydrogen bond for a series of tyrosine kinase inhibitors.[9]

The current study focuses on our initial efforts toward experimentally probing the cooperativity of noncovalent interactions in a systematically varied series of ligands. Thrombin was selected as the model host system because it has a well-defined active site with numerous X-ray structures of ligand complexes available. The basic questions this study addresses are the following: (i) Can a hydrogen bond and a hydrophobic interaction reinforce each other through positive cooperativity? (ii) If yes, then what is the magnitude of the positive cooperativity and can it depend upon the number and type of pre-existing interactions?

Two separate series of thrombin inhibitors were designed. The structural features of the two series and their binding mode in the active site of thrombin are illustrated in Figure 1.

*To whom correspondence should be addressed. For G.K. (for kinetic and the collaborative interpretation of the data): phone, +49 6421 282 1313; fax, +49 6421 282 8994; e-mail, klebe@mailer.uni-marburg.de. For D.G.H. (for the design and synthesis of the compounds, modeling studies, MD simulations, and collaborative interpretation of the data): phone, +1-716-645-4183; fax, +1-716-645-6963; e-mail, hangauer@buffalo.edu.

[a]Abbreviations: NMR, nuclear magnetic resonance; Boc, di-*tert*-butyloxycarbonyl; Fmoc, 9-fluorenylmethyloxycarbonyl; DCM, dichloromethane; DIEA, diisopropylethylamine; DMF, *N*,*N*-dimethylformamide; DMSO, dimethyl sulfoxide; EDCI, 1-(3-dimethylaminopropyl)-3-ethylcarbodiimide hydrochloride; HOBT, hydroxybenzotriazole; HCl, hydrochloric acid; HPLC, high pressure liquid chromatography; HRMS, high resolution mass spectrometry; ITC, isothermal titration calorimetry; LCMS, high pressure liquid chromatography/mass spectrometry; PAB-Z, *N*-benzyloxy-4-aminomethylbenzamidine; Z, benzyloxycarbonyl; MD, molecular dynamics.

 Published on Web 02/11/2010

As shown in Figure 1, the first series has a *m*-chlorobenzyl moiety binding in the S1 pocket. This side chain was selected based upon earlier thrombin inhibitor studies.[10−12] In the second series the *m*-chlorobenzyl moiety is replaced by the more potent benzamidine moiety which forms a salt bridge and two hydrogen bonds with Asp 189 at the bottom of the S1 pocket. While these P1 side chains were held constant within each series, the size of the hydrophobic side chain (R) that binds in the well-defined S3 pocket[13] was systematically increased, from a hydrogen atom to a benzyl group, in the presence or absence of the X = NH_2 that forms a hydrogen bond with the carbonyl oxygen of the Gly 216 residue. In both inhibitor series a proline moiety was selected to bind under Tyr60A and Trp60D in the S2 pocket, as does the natural substrate.[14] If there is no positive cooperativity, then the increased binding affinity per added Å^2 of P3 hydrophobic side chain contact surface would be the same in the absence or presence of the X = NH_2 hydrogen bonding side chain. Furthermore, if the magnitude of the cooperativity depends upon the number and type of pre-existing interactions, then the increased hydrophobic binding affinity in the presence of the X = NH_2 hydrogen bonding side chain could be different for the two series because series II has a salt bridge with two hydrogen bonds in the S1 pocket whereas Series I does not. As described herein the presence of the X = NH_2 hydrogen bond significantly increased the binding affinity per added Å^2 of hydrophobic contact surface and to a somewhat different extent in the two series. Consequently, not accounting for cooperativity of this type in scoring functions could add substantially to the error in predicting binding affinity, since hydrophobic binding is a major component of most ligand−protein complexes, and the error is accumulated over many Å^2 of hydrophobic contact surface.

Series I:

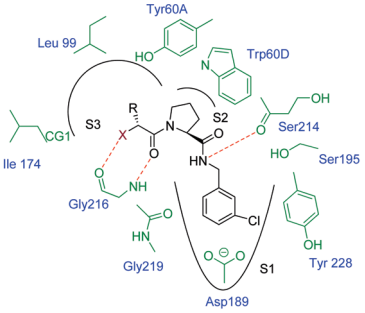

Series I (A): X= -H

Series I (B): X= -NH_2

R = -H, -CH_3, -CH_2CH_3, -$CH(CH_3)_2$, -$CH_2CH(CH_3)_2$, -$C(CH_3)_3$, -$CH_2C(CH_3)_3$*, cyclopentyl, methylcyclopentyl, cyclohexyl, methylcyclohexyl†, benzyl

*only synthesized with X=-NH_2
†only synthesized with X= -H

Series II:

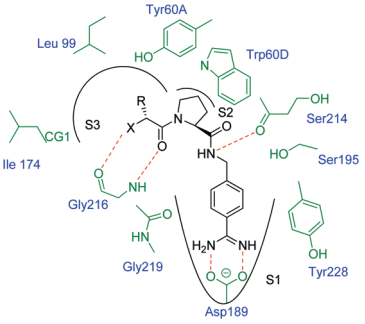

Series II (A): X= -H

Series II (B): X= -NH_2

R = -H†, -CH_3, -CH_2CH_3, -$CH_2(CH_3)_2$, -$CH_2CH_2(CH_3)_2$, -$(CH_3)_3$, -$CH_2(CH_3)_3$*, cyclopentyl†, methylcyclopentyl†, cyclohexyl, methylcyclohexyl†, benzyl

*only synthesized with X=-NH_2

† only synthesized with X= -H

Figure 1. Structural features and binding mode of the designed inhibitors.

Chemistry

Synthesis of Series I. The synthesis of series IA starts with an amide coupling between Boc-proline and *m*-chlorobenzylamine using EDCI/HOBT as the coupling reagents (Scheme 1). The amide **1** was recrystallized from MeOH/water before quantitative Boc-deprotection using methanolic HCl. The amine **2** was then coupled to the different carboxylic acids (Scheme 1) to give products **3a**−**k** or with N-protected D-amino acids (Scheme 2) to give the products (**4a**−**k**). Each product was purified by reverse-phase HPLC. This was followed by the Boc/Fmoc deprotection in case of the amino acids to obtain the final products **5a**−**k**.

Synthesis of Series II. The synthesis of the series II compounds begins with the synthesis of *N*-benzyloxycarbonyl-4-aminomethylbenzamidine **10** as shown in Scheme 3. The synthesis is guided by the process reported by Lila et al.[15] The synthesis begins by conversion of 4-cyanobenzyl bromide to the bis-Boc protected benzylamine **6**. The bromide is displaced with di-*tert*-butyliminodicarboxylate using sodium hydride as a base in anhydrous THF. The cyano compound **6** was converted to the amidoxime **7** by reaction with hydroxylamine. Complete consumption of the starting material was realized when 5 equiv each of DIEA and hydroxylamine hydrochloride were used in refluxing DCM.

Scheme 1. General Scheme for Synthesis of Series IA[a]

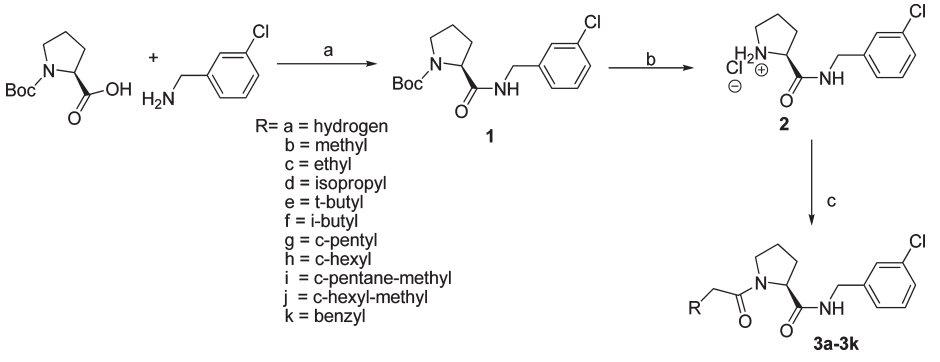

[a] (a) EDCI, HOBT, DIEA, 18 h, 72%; (b) gaseous HCl, ether, 100%; (c) EDCI, HOBT, DIEA, DCM, 12−18 h.

Scheme 2. General Scheme for Synthesis of Series IB[a]

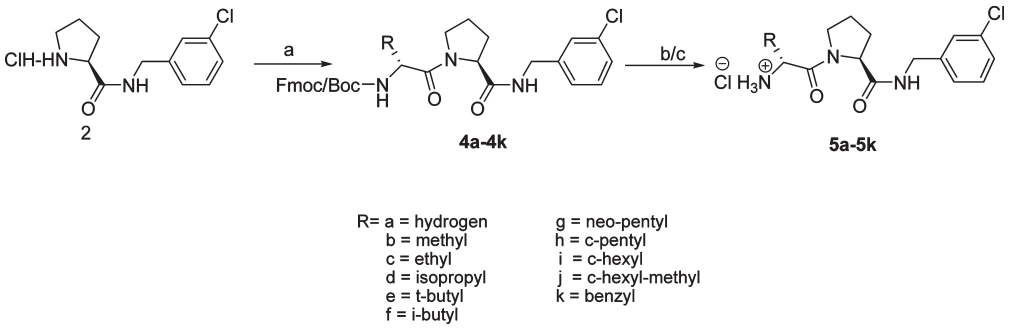

[a] (a) EDCI, HOBT, DIEA, DCM, 12−18 h; (b) gaseous HCl, methanol; (c) 20% piperidine in DCM, 2 h.

Scheme 3. Synthesis of *N*-Benzyloxycarbonyl-4-aminomethylbenzamidine Hydrochloride **10** (PAB-Z·HCl)[a]

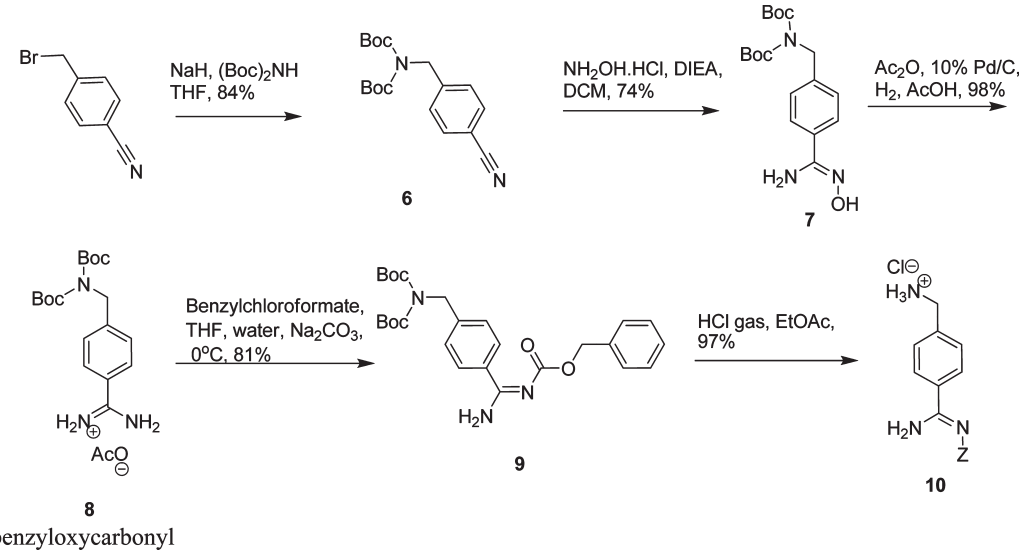

[a] Z = benzyloxycarbonyl.

The recrystallized amidoxime **7** was converted into the free benzamidine by acetylating the hydroxyl group with acetic anhydride and subjecting the resulting acetate to hydrogenolysis over Pd/C in acetic acid. Protection of the benzamidine **8** with a benzyloxycarbonyl group provided **9**. Removal of the Boc groups was achieved with 1 M HCl in methanol to give the hydrochloride salt **10** (PAB-Z·HCl).

An attempt to streamline the synthesis was made by coupling PAB-Z to Boc-L-proline. However, the reaction produced low yields of the coupled product (30−40%) and the need for reverse phase HPLC could not be avoided. Preparation of the dipeptide portion prior to the attachment of the benzamidine was a longer route but proved to be more efficient. A general scheme for the synthesis of this series is shown in Schemes 4 and 5. First, the alkylcarboxylic acids and Boc-D-amino acids are coupled to L-proline benzyl ester for series IIA and IIB, respectively. The ester is then saponified to the carboxylic acid followed by coupling with PAB-Z·HCl. Last, the protecting groups are removed and the product is converted to the hydrochloride salt.

The coupling between L-proline benzyl ester and each of the alkylcarboxylic acids, or Boc-D-amino acids, produced some products that were >95% pure after acid−base workup and carried on to the next step, but others required either crystallization or silica gel chromatography in order to be pure enough to carry forward in the synthesis. The next step was hydrogenation of the benzyl ester and was conducted on a Parr hydrogenator over 10% Pd/C in methanol. The reaction had to be monitored and promptly removed upon completion (2−6 h) to avoid formation of the methyl ester. In most cases the reaction had yields >95% with very good purity. In cases where the methyl ester formed, it was removed by base−acid back-extraction. If needed, the compound was purified using reverse phase HPLC. The next step in the synthesis is the coupling with PAB-Z·HCl. This was performed using EDCI/HOBT with DIEA as the base. DMF was used in place of DCM to increase solubility. The desired products were purified by reverse-phase HPLC. Deprotection of the Z-amidines **13a**−**k** was achieved by catalytic hydrogenation at atmospheric pressure over 10% Pd/C in methanol. The reaction was monitored by LC/MS and typically took between 18 and 36 h to reach completion. The products were converted to the hydrochloride salts with HCl in ether and submitted for biological testing. In the case of **17a**−**h** the intermediate was subjected to Boc-deprotection using methanolic HCl. The mixture was then allowed to stir for 2 h. The solvent was removed to give the desired products as the dihydrochloride salts for biological testing. Further details can be found in the Supporting Information.

Scheme 4. General Scheme for Synthesis of Series IIA[a]

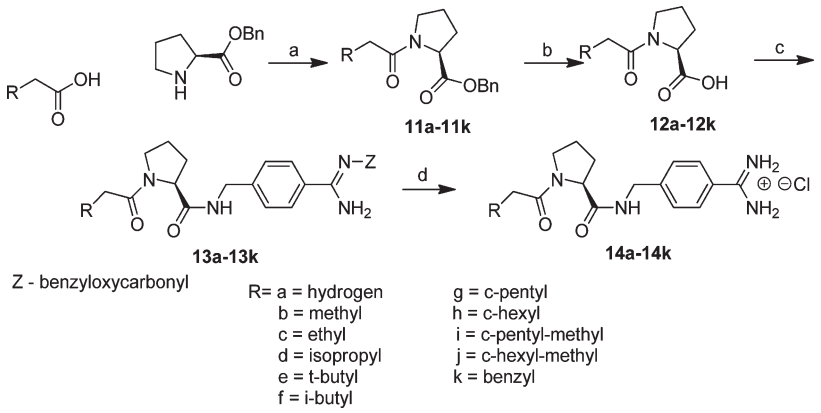

[a] (a) EDCI, HOBT, DIEA, DCM, 12−18 h; (b) H_2/Pd, methanol, 18 h; (c) PAB-Z·HCl, EDCI, HOBT, DIEA, DMF, 12−18 h; (d) H_2/Pd, methanol, 18 h, HCl−methanol, 1 h.

Scheme 5. General Scheme for Synthesis of Series IIB[a]

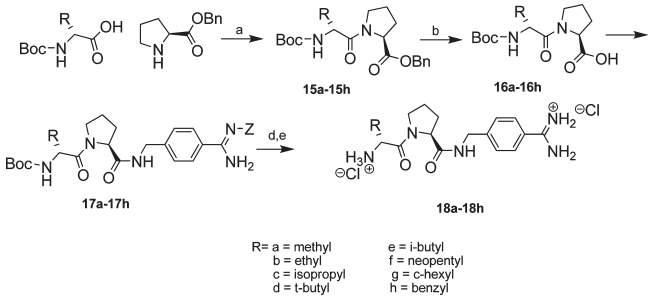

[a] (a) EDCI, HOBT, DIEA, DCM, 12−18 h; (b) H_2/Pd, methanol, 18 h; (c) PAB-Z·HCl, EDCI, HOBT, DIEA, DMF, 12−18 h; (d) H_2/Pd, methanol, 18 h; (e) gaseous HCl, methanol.

Results and Discussion

Binding Affinity and Binding Mode Evaluation. K_i values for compounds **3a**−**k**, **5a**−**k**, **14a**−**k**, and **18a**−**k** binding to thrombin were measured using a standard kinetic photometric assay as described in the Experimental Section. The hydrophobic contact surface areas between the ligands and the active site were calculated using SYBYL 7.3 as described in the Experimental Section. Molecular modeling studies were carried out starting with the crystal structure 1TA2[11] as the starting reference structure for series I. 1TA2 is the crystal structure of thrombin in a complex with an inhibitor similar to **5k**. The only difference between the two ligands is that the inhibitor in the 1TA2 structure has an additional chlorine atom on the phenyl ring that binds in the S1 pocket. For series II, 1K22[13] was used as the starting reference structure. 1K22 is the crystal structure of thrombin in complex with the drug melagatran. The structure of this drug is similar to that of **18g**. The only difference between the two is that melagatran has a four-membered ring in the central S2 pocket instead of the five-membered ring in **18g** and acetic acid is attached to the terminal amine.

The modeling studies were carried out by replacing the additional chlorine atom in 1TA2 with a hydrogen atom for series I or replacing the four-membered ring in the central S2 pocket with a five-membered proline ring and deleting the terminal acetic acid in 1K22 for series II. For both series the P3 side chain was modified to correspond to the designed inhibitors (**3a**−**k**, **5a**−**k**, **14a**−**k**, and **18a**−**h**). The resulting modeled complexes were minimized to convergence using the SYBYL force field. Once the optimized geometry was obtained, the hydrophobic contact surface area was calculated. The detailed procedure used for the calculation of the hydrophobic contact surface area is described in the Experimental Section.

Table 1. Series I K_i Values and Corresponding ΔG Values for Binding, and Hydrophobic Contact Surface Area As Obtained from Molecular Modeling

compd	K_i (μM)	±sd	ΔG (kJ/mol)	±sd	hydrophobic contact surface area (Å^2)	±sd
3a	1.46×10^3	409	−16.2	1.68	292	3.76
3b	444	133	−19.1	0.69	311	2.59
3c	322	190	−19.9	0.01	334	2.02
3d	155	86.0	−21.7	0.68	342	1.36
3e	484	139	−18.9	0.26	342	1.15
3f	109	46.3	−22.6	0.72	365	1.62
3g	72.4	22.1	−23.6	0.26	368	2.20
3h	34.5	6.34	−25.5	0.73	380	0.81
3i	92.9	11.0	−23.0	0.41	400	1.66
3j	29.7	7.45	−25.8	0.57	391	2.27
3k	94.3	34.3	−23.0	0.65	384	0.65
5a	8.08	4.22	−29.1	0.59	299	0.47
5b	33.0	11.8	−25.6	0.20	312	0.74
5c	6.81	1.60	−29.5	0.38	334	1.33
5d	2.54	0.66	−31.9	0.47	342	1.24
5e	0.92	0.28	−34.5	0.38	338	1.88
5f	0.54	0.19	−35.8	0.86	368	1.58
5g	0.41	0.10	−36.5	0.39	378	1.94
5h	0.43	0.06	−36.3	0.36	370	0.85
5i	0.15	0.11	−39.0	0.79	384	1.82
5j	0.10	0.04	−39.9	0.88	409	0.76
5k	0.18	0.15	−38.5	0.96	387	0.40

The experimentally obtained K_i values, the corresponding calculated Gibbs energy of binding, and the calculated hydrophobic contact surface areas for series I and II are listed in Tables 1 and 2, respectively.

The Tables 1 and 2 data for the inhibitor series I and II are plotted in Figure 2a and Figure 2b, respectively. Four important observations and data interpretations can be made from these plots:

(1) Both series produce a linear correlation between the improvement in the ΔG of binding and the increase in hydrophobic contact surface in the S3 pocket, in the presence and absence of the additional hydrogen bond (X = H or NH_2, respectively). This suggests that any cooperativity that

Table 2. Series II K_i Values and Corresponding ΔG Values, and Hydrophobic Contact Surface Area As Obtained from Molecular Modeling

compd	K_i (μM)	±sd	ΔG (kJ/mol)	±sd	hydrophobic contact surface area (Å^2)	±sd
14a	56.1	8.28	−24.3	0.35	287	0.21
14b	39.0	13.8	−25.2	0.85	303	2.01
14c	5.70	1.19	−29.9	0.47	323	0.69
14d	3.81	0.57	−30.9	0.35	354	3.88
14e	0.94	0.33	−34.4	0.75	364	2.76
14f	1.28	0.27	−33.6	0.51	365	2.85
14g	1.64	0.28	−33.0	0.40	367	2.40
14h	3.61	0.53	−31.1	0.33	374	2.43
14i	1.18	0.30	−33.8	0.86	387	2.74
14j	1.17	0.41	−33.9	0.53	393	2.34
14k	0.75	0.19	−35.0	0.77	380	0.60
18a	1.42	0.24	−33.4	0.40	304	1.56
18b	0.18	0.03	−38.5	0.42	322	0.98
18c	0.07	0.03	−41.0	0.99	333	0.04
18d	0.15	0.02	−39.0	0.31	328	3.26
18e	0.02	0.02	−43.5	1.17	365	3.17
18f	0.011	0.002	−45.5	0.46	355	2.82
18g	0.023	0.006	−43.7	0.71	377	0.37
18h	0.004	0.001	−47.9	1.34	365	0.30

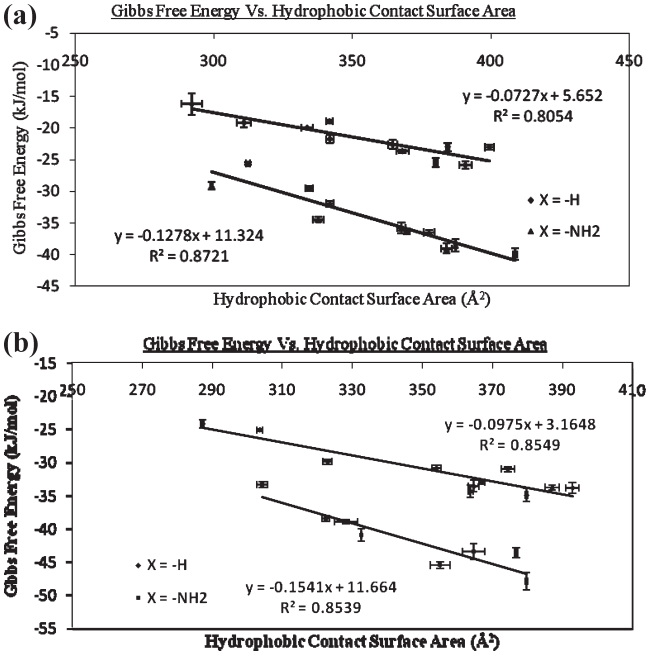

Figure 2. (a) Plot of binding Gibbs energy vs hydrophobic contact surface area for series I (A) and series I (B). (b) Plot of binding Gibbs energy vs hydrophobic contact surface area for series II (A) and series II (B). The error in the two slopes was obtained by fitting the data to a linear regression model using WinNonLin Professional. The Student's t test was also performed on the two slopes to confirm that the values were outside experimental error ($P < 0.01$).

is present between the hydrophobic R side chain and the hydrogen bonding X side chain does not change in magnitude as the R side chain increases in size to fill the S3 pocket.

(2) The slope of the line for the series IB, with an added hydrogen bond (X = NH_2), is −0.128 (kJ/mol)/Å^2 of hydrophobic contact surface area added, which is 75% more than that of −0.073 (kJ/mol)/Å^2 for the series IA compounds lacking the added hydrogen bond (X = H). This demonstrates that the presence of the adjacent hydrogen bond would require a scoring function to award almost twice as much binding affinity for each Å^2 of hydrophobic contact surface in the S3 pocket.

(3) The slope of the line for series IIB, with an added hydrogen bond (X = NH_2), is −0.154 (kJ/mol)/Å^2 of hydrophobic contact surface area added, which is 59% more than −0.097 (kJ/mol)/Å^2 for series IIA lacking the added hydrogen bond (X = H). The series IIB vs series IIA data confirm the trend obtained with series IB vs series IA but also suggests that the presence of the benzamidine salt bridge in series II, with a bifurcated hydrogen bonding to Asp 189 in the S1 pocket, may somewhat dampen the cooperativity between the P3 hydrophobic side chain and the adjacent hydrogen bond when X = NH_2.

(4) The presence of additional strong interactions elsewhere in the complex may be expected to help position the hydrophobic side chain in the S3 pocket so that the binding affinity will not be enhanced as much with the installation of another hydrogen bond immediately adjacent to it. This concept is supported by comparing the binding affinity enhancement −0.097 (kJ/mol)/Å^2 of added hydrophobic contact surface in the S3 pocket in the presence of the benzamidine hydrogen bonds/salt bridge in the S1 pocket (series IIA, X = H) to the −0.073 (kJ/mol)/Å^2 for the series IA compounds (X = H) lacking any hydrogen bonding/salt bridge in the S1 pocket. These data suggest that the presence of the benzamidine hydrogen bonds/salt bridge in the S1 pocket has already accomplished some of the P3 side chain positioning such that a 33% increase in the strength of the hydrophobic interaction in the S3 pocket occurs. This indicates that cooperativity between hydrogen bonds/salt bridges and hydrophobic interactions can also be long-range, albeit with a dampened magnitude. The cooperativity between the adjacent hydrogen bond (X = NH_2) and the hydrophobic binding in the S3 pocket was 75% for series I and is reduced to 33% when the hydrogen bonds/salt bridge are installed in the S1 pocket (benzamidine) instead of immediately adjacent to the P3 hydrophobic side chain. When the hydrogen bond is already present adjacent to the P3 side chains, and we add the S1 pocket benzamidine hydrogen bonds/salt bridge (i.e., series IB, X = NH_2 to series IIB, X = NH_2), the long-range cooperativity is further reduced to 21% (−0.128 to −0.154 (kJ/mol)/Å^2, respectively) from 33%. This suggests that the magnitude of cooperativity is dependent not only upon the distance between the interacting side chains but also upon how much ligand positioning has already been accomplished by pre-existing hydrogen bonds. These interpretations are also supported by the molecular dynamics results discussed later.

A linear correlation between the Gibbs energy of binding and hydrophobic contact surface area was previously reported for buried hydrophobic residues at the interface in a protein−protein interaction.[16] The protein interface stabilization free energy (slope) was reported to improve by −0.0627 ± 0.005 kJ/mol upon burial of each additional Å^2 of hydrophobic surface, comparable to the −0.073 ± 0.006 (kJ/mol)/Å^2 obtained for series I in the current study when the adjacent hydrogen bond was absent (X = H). The values obtained in the current study with ligand−thrombin interactions and in the protein−protein interaction study[16] are in the range of the values reported in the literature

(0.08−0.20 (kJ/mol)/Å^2) for hydrophobic interactions in a ligand−receptor complex.[17] The current study suggests that this 2.5-fold range may be at least partially due to the presence or absence of cooperative interactions when the ΔG values for the hydrophobic interactions were measured.

To put into perspective the potential underestimate of binding affinity for not including positive cooperativity, one can consider that the larger P3 side chain ligands in the current study have about 400 Å^2 of hydrophobic contact surface compared to about 300 Å^2 of hydrophobic contact surface when there is no P3 side chain. If a scoring function were to calculate the difference in the binding affinity based upon −0.073 (kJ/mol)/Å^2 instead of the correct −0.128 (kJ/mol)/Å^2 (when X = NH_2) for series I, then the calculated K_i would be underestimated by about an order of magnitude.

The data can also be analyzed using double functional group replacement cycles as illustrated in Figure 3. These cycles for the indicated series of inhibitors show that the X = NH_2 group and benzyl P3 side chain have a positive cooperativity of 5.97 kJ/mol for series I (Figure 3a). Similar analysis for series II (Figure 3b) again indicates positive cooperativity (4.37 kJ/mol) but somewhat smaller than for series I.

In order to validate our modeling results, the thrombin complex crystal structures with compounds **5c** (small side chain) and **5k** (large side chain) from series I and with compounds **14c**, **18b** (small side chain) and **14k**, **18h** (large side chain) from series II were solved.[15] The bound inhibitor geometries obtained from these crystal structures were compared with the geometries obtained from the modeling. Figure 4 shows the modeled inhibitor geometries superimposed upon the corresponding crystal structure geometries. As shown, the modeled geometries are essentially identical to that obtained from the crystal structures, which confirms that the averaged binding modes obtained from crystal analysis and modeling agree well. This indicates that the modeled complexes and the corresponding calculated hydrophobic contact surfaces are valid.

Crystal structures for the compounds from series I which lack the additional hydrogen bond (X = H) could not be obtained because of the weaker binding affinity of the compounds in this series. However, crystal structures were successfully determined when X = H for series II (compounds **14c** and **14k**). On the basis of the close correspondence that was obtained with series II for the crystallographic and modeled P3 side chains when X = NH_2, and the modeled and crystallographic P3 side chains when X = H,[18] it was assumed that the modeled geometry obtained for series I with X = H is also relevant.

With this first experimental demonstration of how significantly hydrophobic binding strength can vary because of neighboring interactions, the question now becomes "What is the cause of this?" As indicated earlier a possible explanation for the increase in the binding affinity per Å^2 of hydrophobic contact surface in the presence of the additional hydrogen bond is the likely restriction of P3 side chain movement inside the hydrophobic S3 pocket. This restriction could cause the side chain to spend more time in proximity to the hydrophobic S3 pocket surface and thereby potentially enhance the associated van der Waals interactions. A second possibility is that as the P3 side chain is increased in size, the reduction in ligand residual motion (due to a complementary steric filling of the S3 pocket) may result in a strengthening of

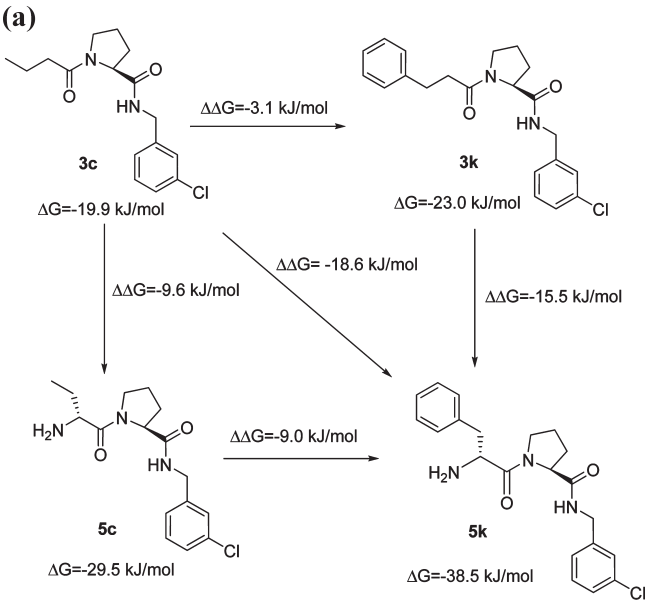

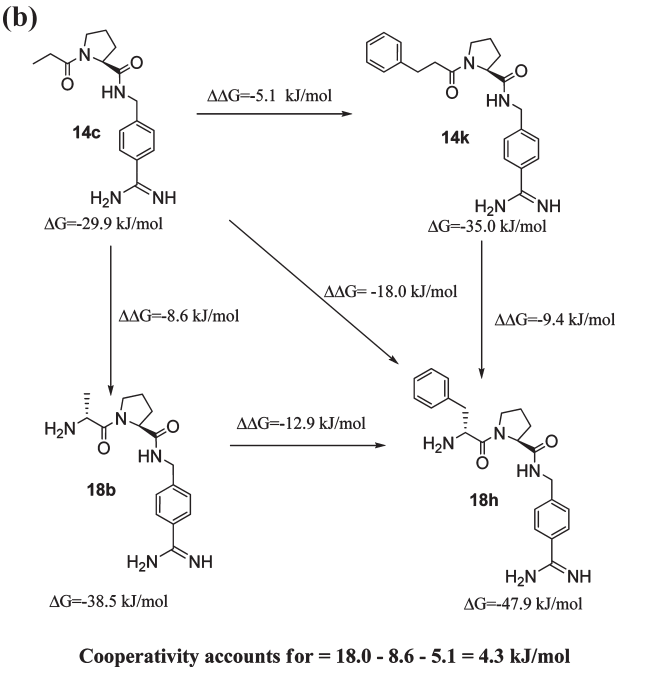

Figure 3. (a) Double functional group replacement cycle demonstrating positive cooperativity for series I. (b) Double functional group replacement cycle demonstrating positive cooperativity for series II.

the hydrogen bond between the terminal NH_2 and the Gly 216 residue. However, in order to be consistent with the linear correlation shown in Figure 2, the improvement in the strength of this hydrogen bond would need to be linearly dependent upon the gradual increase in hydrophobic contact surface in the S3 pocket as the side chain size is increased. In order to gain further insight into these two possibilities, molecular dynamics (MD) simulations were performed on select inhibitors in each series. The P3 isopropyl side chain derivatives were selected as examples with a small hydrophobic side chain because crystal structure analyses showed that the S3 pocket accommodates bound water molecules, in addition to the hydrophobic side chain, with side chains

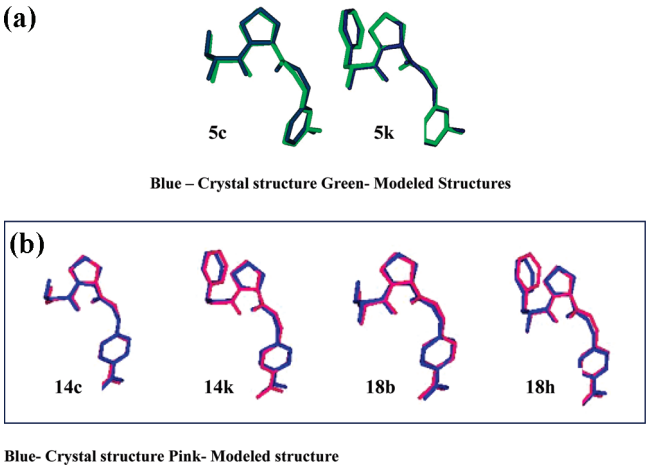

Figure 4. (a) Overlay of crystal vs modeled inhibitors for series I. (b) Overlay of crystal vs modeled inhibitors for series II.

smaller than the isopropyl group.[18] These co-occupancy water molecules add a complication to the relative interpretation of the MD simulations, since they are not present with the larger side chains that are used in the comparison. Consequently, we selected compounds **3d** and **5d** (series I, *m*-chlorobenzyl) and **14d** and **18c** (series II, benzamidine), all of which contain a P3 isopropyl side chain, as an example of a small alkyl group for the MD simulations (Figure 5a). The benzyl group was selected as the large P3 side chain so that compounds **3k** and **5k** (series I, *m*-chlorobenzyl) and **14k** and **18h** (series II, benzamidine) were utilized for the large side chain MD simulations (Figure 5b). The detailed procedure of the MD simulations is described in the Experimental Section. An analysis of the trajectory over 1 ns revealed interesting differences in the two series as illustrated in Figure 6. Table 3 summarizes the corresponding average distances in Å between the P3 hydrophobic side chains and CD1 of the adjacent Leu 99 residue at the back of the S3 pocket, as well as the average hydrogen bond distance between the terminal amino group and Gly 216.

In Figure 6a the distances between the centroid of the isopropyl side chain of compounds **3d**, **5d** (X = H, NH_2) and **14d**, **18c** (X = H, NH_2) of series I and II, respectively, and CD1 of the adjacent Leu 99 residue at the edge of the S3 pocket are shown. Figure 6b shows the corresponding distance for the corresponding benzyl derivatives **3k**, **5k** and **14k**, **18h**. Along the trajectories for these eight compounds it is observed that the distance from the P3 side chain to the S3 pocket wall only fluctuates by an average of ±0.38 Å across both series (Table 3), which indicates that these side chains remain inside the hydrophobic S3 pocket even in the absence of the additional hydrogen bond. Also, the isopropyl and benzyl side chains (small and large) spend more time closer to the Leu 99 residue located in the S3 pocket in the presence of the additional hydrogen bond than in its absence for both series I and II. This suggests that the hydrogen bond strengthens the hydrophobic interaction of the attached side chain. However, the average distance between the hydrophobic side chain and the Leu 99 residue in the absence of the additional hydrogen bond for series II is smaller than for series I. This is probably due to the presence of the benzamidine moiety which forms a hydrogen bonding salt bridge with Asp 189 in the S1 pocket, thereby already reducing the residual entropy of the inhibitor somewhat as indicated

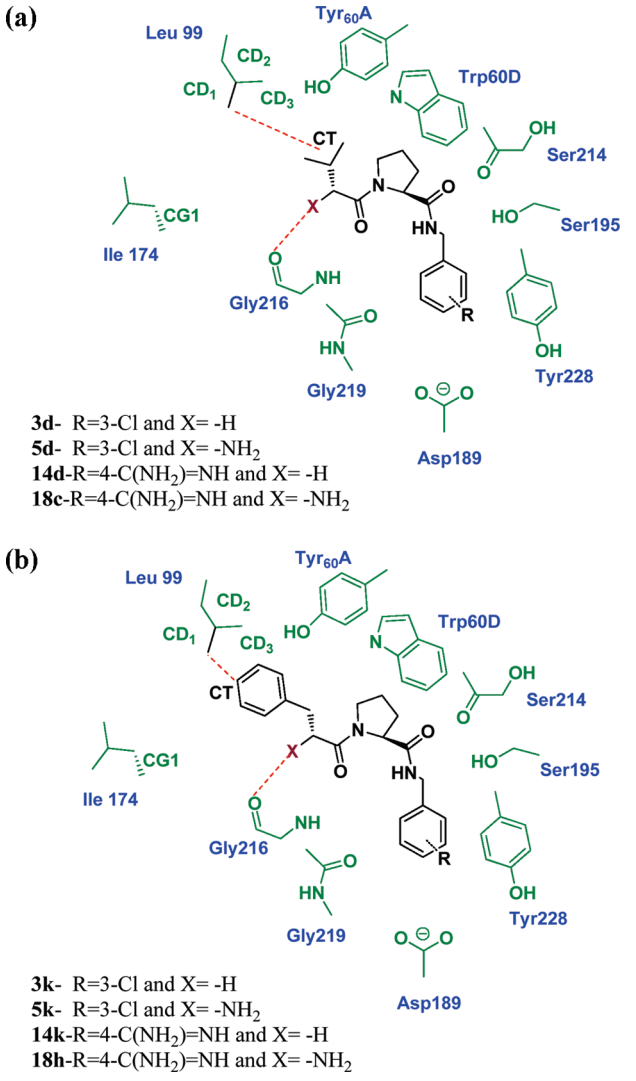

Figure 5. Schematic drawing of the binding mode of the inhibitors with isopropyl side chain (a) and benzyl side chain (b) in S3 pocket. The distances recorded along the molecular dynamics trajectory are shown as dotted lines.

earlier. Hence, the installation of an additional hydrogen bond in series II does not reduce the residual motion of the inhibitors as much as in series I.

The hydrogen bond distance between the terminal NH_2 and the Gly 216 carbonyl oxygen atom was also monitored over 1 ns for compounds **5d**, **5k** and **18c**, **18h**, and the results are illustrated in Figure 6c. This MD simulation suggests that the larger side chains in the S3 pocket reduce the time-average length of the hydrogen bond and thus the strength.

Overall the MD simulation data suggest the following:

(1) The additional hydrogen bond to Gly 216 (X = NH_2) holds the P3 side chains closer to the wall of the hydrophobic pocket for series I and II, most likely resulting in the additional binding free energy per $Å^2$ of hydrophobic contact surface area. For series I (*m*-Cl) the time-averaged mean hydrophobic side chain distance to the S3 pocket wall decreased by 1.57 and 0.49 Å for the small (isopropyl) and large (benzyl) side chains, respectively, when the Gly 216 hydrogen bond is installed (X = NH_2). For series II (benzamidine) the corresponding mean side chain distance decreases are reduced to 0.71 and 0.39 Å, respectively.

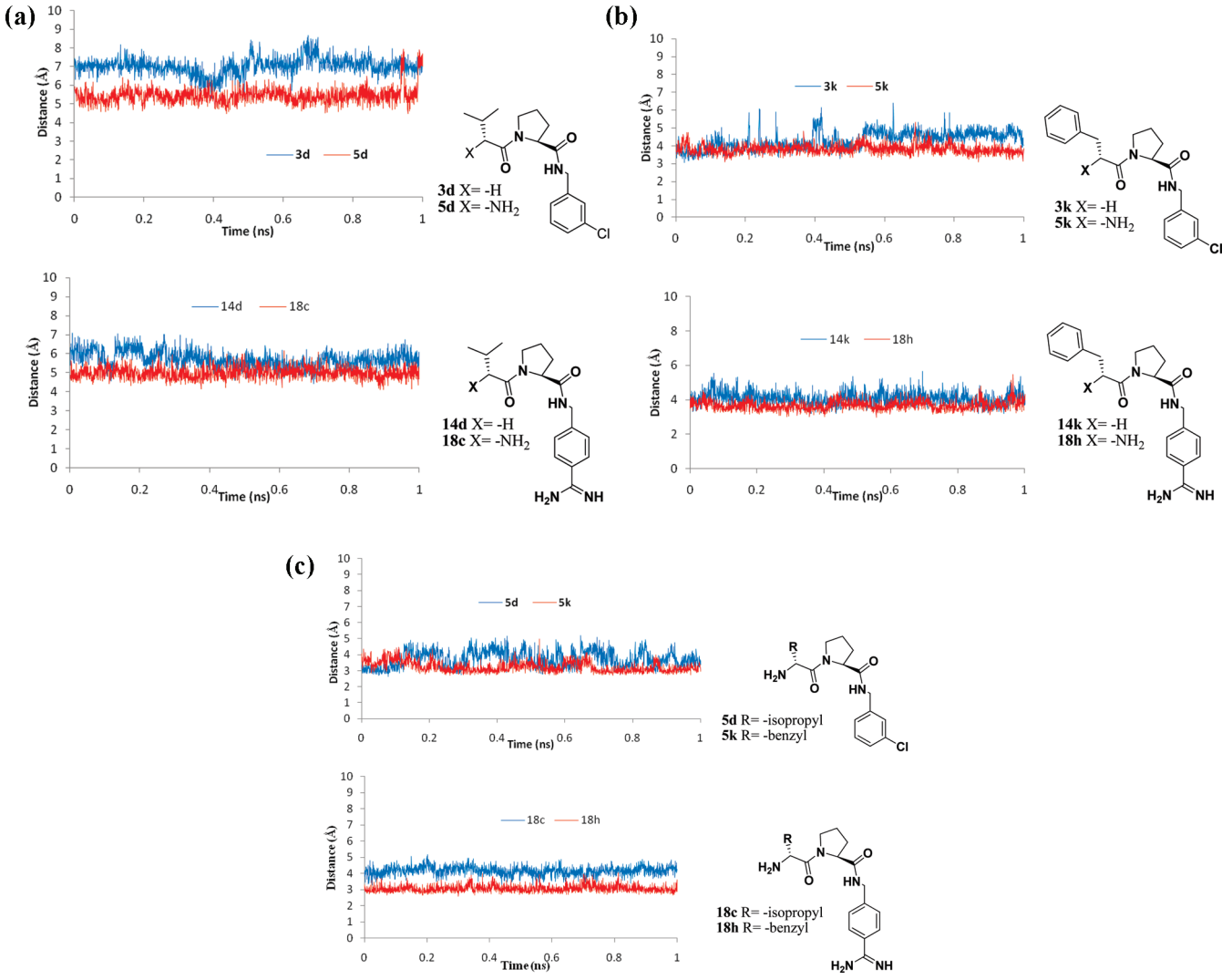

Figure 6. Distances recorded along the molecular dynamics trajectory: (a) fluctuations of representative distances over 1 ns from the centroid of the inhibitor side chain to CD1 of Leu 99; (b) fluctuations of representative distances over 1 ns from the terminal atom of the benzyl side chain to CD1 of Leu99; (c) fluctuations of representative distances over 1 ns from terminal amine of the inhibitor to the carbonyl oxygen of Gly 216.

Table 3. Average Distances in Å between the Hydrophobic Side Chain and CD1 of the Adjacent Leu99 Residue at the Back of the S-3 Pocket and the Average Hydrogen Bond Distance between the Terminal Amine and Gly 216 Recorded over 1 ns

compd	time averaged distance between inhibitor side chain centroid/ terminal atom CT to Leu99 (Å)	±sd	average H-bond distance (Å)	±sd
3d	7.02	0.45		
3k	4.31	0.49		
5d	5.45	0.44	3.73	0.52
5k	3.82	0.27	3.24	0.33
14d	5.70	0.43		
14k	4.08	0.37		
18c	4.99	0.31	4.17	0.27
18h	3.69	0.26	3.06	0.21

(2) The presence of the benzamidine S1 pocket hydrogen bonding salt bridge has already reduced the distance of the side P3 side chain to the S3 pocket wall. The small (isopropyl) and large (benzyl) side chains are closer to the S3 pocket wall by 1.32 and 0.23 Å for the benzamidine compounds **14d** and **14k** compared to the corresponding *m*-Cl compounds **3d** and **3k**, respectively, all of which lack the hydrogen bond to Gly 216 (X = H). When the hydrogen bond to Gly 216 is present (X = NH_2), then the small (isopropyl) and large (benzyl) side chains are positioned closer to the S3 pocket wall by 0.46 and 0.13 Å for the benzamidine compounds **18c** and **18h** compared to the corresponding *m*-Cl compounds **5d** and **5k**, respectively. However this closer positioning is less dramatic than in the absence of the hydrogen bond to Gly 216. This again suggests that the presence of the benzamidine hydrogen bonding in the S1 pocket has already accomplished some of the close P3 side chain positioning that the X = NH_2 hydrogen bond to Gly 216 can provide so that adding the hydrogen bond to Gly 216 is less beneficial to binding in the benzamidine series compared to the *m*-Cl series.

(3) The hydrogen bond appears to get shorter and stronger as the size of the hydrophobic side chain increases. For the *m*-Cl series and the benzamidine series the hydrogen bond to Gly 216 shortens by 0.49 and 1.11 Å when the side chain is increased from isopropyl to benzyl (from **5d** to **5k** and from **18c** to **18h**, respectively).

(4) When one compares the standard deviations of the distances along the MD trajectory for the key interactions (Table 3), suggestions regarding the residual motion of these interactions emerge. Upon installation of the hydrogen bond to Gly 216 in the *m*-Cl series I P3 isopropyl side

inhibitor (**3d** vs **5d**), the standard deviation of the hydrophobic contact distance does not change significantly (±0.45 to 0.44 Å) even though the average distance to the S3 pocket wall is reduced from 7.02 to 5.45 Å. On the other hand when this hydrogen bond is installed in the benzamidine series II P3 isopropyl side chain inhibitor (**14d** to **18c**), the analogous standard deviations are reduced by ±0.12 Å (±0.43 to 0.31 Å) while the distance to the S3 pocket wall is reduced from 5.70 to 4.99 Å. This comparison indicates that as the P3 isopropyl side chain is moved closer to the S3 pocket wall the residual motion of the side chain is decreased. When the analogous comparisons are made with the larger P3 benzyl side chain in the *m*-Cl series I (**3k** vs **5k**), the standard deviation of the hydrophobic contact distance now decreases by a more significant ±0.22 Å (±0.49 to 0.27 Å) while the distance to the S3 pocket wall is reduced from 4.31 to 3.82 Å. In the benzamidine series II with the P3 benzyl side chain (**14k** vs **18h**) the standard deviation of the hydrophobic contact distance decreases by ± 0.11 Å (±0.37 to 0.26 Å) while the distance to the S3 pocket wall is reduced from 4.08 to 3.69 Å. This comparison analogously indicates that as the P3 benzyl side chain is moved closer to the S3 pocket wall, the residual motion of the side chain is decreased. Finally, the effect of the size of the P3 side chain on the standard deviation of the hydrogen bond to Gly 216 can be analyzed from the data in Table 3. In the *m*-Cl series I increasing the P3 side chain from an isopropyl group to a benzyl group (**5d** to **5k**) reduces the standard deviation of the hydrogen bond to Gly 216 by ±0.19 Å (±0.52 to 0.33 Å) while the hydrogen bonding distance decreases from 3.73 to 3.24 Å. In the benzamidine series II increasing the P3 side chain from an isopropyl group to a benzyl group (**18c** to **18h**) reduces the standard deviation of the hydrogen bond to Gly 216 by ±0.06 Å (±0.27 to 0.21 Å) while the hydrogen bonding distance decreases from 4.17 to 3.06 Å. This comparison indicates that increasing the size of the P3 side chain both shortens the length of the hydrogen bond to Gly 216 and reduces the residual motion along the hydrogen bond.

Conclusions

This study demonstrates that the presence of a hydrogen bond adjacent to an inhibitor's hydrophobic side chain can mutually increase the strength of these interactions compared to what would be expected based upon simple additivity. This increase in strength is suggested to be due to the hydrogen bond holding the hydrophobic side chains closer and more firmly against the hydrophobic pocket wall and conversely the side chain increasing the strength of the hydrogen bond due to stabilizing its geometry. Thus, a hydrophobic interaction and the hydrogen bond can mutually reinforce each other. The data also demonstrate that cooperativity between hydrophobic interactions and hydrogen bonds can be longer range, albeit with reduced amplitude, extending from the thrombin S1 pocket to the S3 pocket. Finally, the magnitude of the cooperativity between the adjacent hydrogen bond and the hydrophobic interaction in the S3 pocket was shown to be reduced in the presence of additional hydrogen bonds/salt bridge in the S1 pocket. To the best of our knowledge, this is the first in-depth experimental demonstration of cooperativity between hydrophobic interactions and hydrogen bonds in protein−ligand complexes. The results obtained suggest that scoring function predictions of ligand binding affinities could be improved if cooperativity were included. The potential error in binding affinity predictions for not including cooperativity between a typical hydrophobic side chain of 100 $Å^2$ contact surface and an adjacent hydrogen bond can be about an order of magnitude.

Experimental Section

Molecular Modeling. All modeling experiments were performed using SYBYL software (Tripos, St. Louis, MO), versions 6.9 or 7.0, on an HP or SGI workstation. Each modeling experiment used thrombin coordinates downloaded from the Brookhaven Web site (www.rcsb.org) as described earlier. It was observed that the thrombin crystal structure is essentially unchanged with the various inhibitor complexes evaluated in this study.[15] Hydrogens were added, and charges were computed using the Gasteiger−Marsilli protocol. The ligand was extracted from the binding site, and the inhibitors discussed herein were manually constructed and docked using analogous thrombin inhibitor crystal structures as a guide. The complexes were minimized to convergence while holding the protein fixed, using the Tripos force field and the default parameters with the exception of using a dielectric constant of 80.0.

Calculation of Hydrophobic Contact Surface Area. Once the energy minimized binding mode is obtained using the above procedure, the MOLCAD surface is generated for the protein. This surface is first mapped according to lipophilic potential. Only the hydrophobic surface is used for the analysis. In order to do so, the midpoint of the lipophilic potential range for the protein was calculated within SYBYL and the potential from the midpoint to the maximally lipopholic surface was defined as the protein lipophilic surface. The next step is to take the distance between the protein and the ligand into account. In order to do so, the protein MOLCAD surface is mapped again except this time according to the distance between the ligand and the protein. A new MOLCAD protein surface is then created that satisfies both criteria: (1) It has a lipophilic potential from the midpoint of the lipophilic scale to the maximum value, and (2) it has a distance between the ligand (including hydrogens) and the protein of 2.6 Å or less so that a water molecule cannot be accommodated between the two surfaces (diameter of water, 2.8 Å). The hydrophobic protein surface area that meets both criteria is then calculated. The above procedure is repeated three times in order to obtain an average measurement of the contact surface area and a standard deviation.

Molecular Dynamics Simulations. The protein−ligand complexes were placed in a sphere of TIP3 water molecules of radius 50 Å, about 50 000 atoms. For the ligands the Amber GAFF force field was used. The atomic charges of the ligands were calculated by fitting (program RESP) to the HF/6-31G* electrostatic potential (Gaussian 98) based on the crystallographically observed conformation. The MD was started by heating the solvent to 300 K over a period of 20 ps and cooling to 100 K over a period of 5 ps, keeping the solute fixed. Then the system was gradually brought to 300 K over 25 ps. The simulation was carried on for 1050 ps under constant temperature and pressure (NPT), applying periodic boundary conditions (Amber, version 8.0). Energy data were stored every 10 time steps, solute coordinates every 0.5 ps, and solvent coordinates every 5 ps. All results presented refer to the 1 ns trajectories, excluding the first 1 ns required for temperature adjustment and equilibration (an equilibrated state with respect to the total potential energy in the system was reached after 100 ps). Analyses were carried out primarily using modules from the Amber program suite, while VMD[19] and DS Viewer Pro (http://accelrys.com/products) were used for visualization purposes.

Biological Assay. Kinetic inhibition of human thrombin (from Beriplast, CSL Behring, Marburg, Germany) was determined photometrically at 405 nm using the chromogenic substrate Pefachrom tPa (LoxoGmbH, Dossenheim, Germany) according to the protocols described by Stürzebecher et. al.[20]

under the following conditions: 50 mM Tris/HCl, pH 7.4, 154 mM NaCl, 5% DMSO, 0.1% PEG 8000 at 25 °C using different concentrations of substrate and inhibitor. K_i values ($n \geq 3$) were determined as described by Dixon.[21]

Acknowledgment. We kindly acknowledge CSL Behring, Marburg, Germany, for supplying us with generous amounts of human thrombin from production of Beriplast. L.M., M.S., M.F., and D.G.H. contributed the design and synthesis of the compounds, the modeling studies, and the MD simulations, as well as collaborative interpretation of the data. B.B., A.H., and G.K. contributed to the kinetic and the collaborative interpretation of the data.

Supporting Information Available: Experimental details for the synthesis of all the compounds. This material is available free of charge via the Internet at http://pubs.acs.org.

References

(1) Whitesides, G. M.; Krishnamurthy, V. M. Designing ligands to bind proteins. *Q. Rev. Biophys.* **2005**, *38*, 385–395.
(2) Warren, G. L.; Andrews, C. W.; Capelli, A. M.; Clarke, B.; LaLonde, J.; Lambert, M. H.; Lindvall, M.; Nevins, N.; Semus, S. F.; Senger, S.; Tedesco, G.; Wall, I. D.; Woolven, J. M.; Peishoff, C. E.; Head, M. S. A critical assessment of docking programs and scoring functions. *J. Med. Chem.* **2006**, *49*, 5912–5931.
(3) Hubbard, R. E. 3D structure and the drug-discovery process. *Mol. BioSyst.* **2005**, *1*, 391–406.
(4) Talhout, R.; Villa, A.; Mark, A. E.; Engberts, J. B. Understanding binding affinity: a combined isothermal titration calorimetry/molecular dynamics study of the binding of a series of hydrophobically modified benzamidinium chloride inhibitors to trypsin. *J. Am. Chem. Soc.* **2003**, *125*, 10570–10579.
(5) Nguyen, B.; Neidle, S.; Wilson, W. D. A role for water molecules in DNA−ligand minor groove recognition. *Acc. Chem. Res.* **2009**, *42*, 11–21.
(6) Dill, K. A. Additivity principles in biochemistry. *J. Biol. Chem.* **1997**, *272*, 701–704.
(7) Williams, D. H.; Searle, M. S.; Mackay, J. P.; Gerhard, U.; Maplestone, R. A. Toward an estimation of binding constants in aqueous solution: studies of associations of vancomycin group antibiotics. *Proc. Natl. Acad. Sci. U.S.A.* **1993**, *90*, 1172–1178.
(8) Williams, D. H.; Stephens, E.; O'Brien, D. P.; Zhou, M. Understanding noncovalent interactions: ligand binding energy and catalytic efficiency from ligand-induced reductions in motion within receptors and enzymes. *Angew. Chem., Int. Ed.* **2004**, *43*, 6596–6616.
(9) Lafleur, K.; Huang, D.; Zhou, T.; Caflisch, A.; Nevado, C. Structure-based optimization of potent and selective inhibitors of the tyrosine kinase erythropoietin producing human hepatocellular carcinoma receptor B4 (EphB4). *J. Med. Chem.* **2009**, *52*, 6433–6446.
(10) Lumma, W. C., Jr.; Witherup, K. M.; Tucker, T. J.; Brady, S. F.; Sisko, J. T.; Naylor-Olsen, A. M.; Lewis, S. D.; Lucas, B. J.; Vacca, J. P. Design of novel, potent, noncovalent inhibitors of thrombin with nonbasic P-1 substructures: rapid structure−activity studies by solid-phase synthesis. *J. Med. Chem.* **1998**, *41*, 1011–1013.
(11) Tucker, T. J.; Brady, S. F.; Lumma, W. C.; Lewis, S. D.; Gardell, S. J.; Naylor-Olsen, A. M.; Yan, Y.; Sisko, J. T.; Stauffer, K. J.; Lucas, B. J.; Lynch, J. J.; Cook, J. J.; Stranieri, M. T.; Holahan, M. A.; Lyle, E. A.; Baskin, E. P.; Chen, I. W.; Dancheck, K. B.; Krueger, J. A.; Cooper, C. M.; Vacca, J. P. Design and synthesis of a series of potent and orally bioavailable noncovalent thrombin inhibitors that utilize nonbasic groups in the P1 position. *J. Med. Chem.* **1998**, *41*, 3210–3219.
(12) Baum, B.; Mohamed, M.; Zayed, M.; Gerlach, C.; Heine, A.; Hangauer, D.; Klebe, G. More than a simple lipophilic contact: a detailed thermodynamic analysis of nonbasic residues in the s1 pocket of thrombin. *J. Mol. Biol.* **2009**, *390*, 56–69.
(13) Dullweber, F.; Stubbs, M. T.; Musil, D.; Sturzebecher, J.; Klebe, G. Factorising ligand affinity: a combined thermodynamic and crystallographic study of trypsin and thrombin inhibition. *J. Mol. Biol.* **2001**, *313*, 593–614.
(14) Stubbs, M. T.; Oschkinat, H.; Mayr, I.; Huber, R.; Angliker, H.; Stone, S. R.; Bode, W. The interaction of thrombin with fibrinogen. A structural basis for its specificity. *Eur. J. Biochem.* **1992**, *206*, 187–195.
(15) Lila, C.; Gloanec, P.; Cadet, L.; Hervé, Y.; Fournier, J.; Leborgne, F.; Verbeuren, T. J.; De Nanteuil, G. Large-scale preparation of protected 4-aminomethylbenzamidine. Application to the synthesis of the thrombin inhibitor, melagatran. *Synth. Commun.* **1998**, *28*, 4419–4429.
(16) Vallone, B.; Miele, A. E.; Vecchini, P.; Chiancone, E.; Brunori, M. Free energy of burying hydrophobic residues in the interface between protein subunits. *Proc. Natl. Acad. Sci. U.S.A.* **1998**, *95*, 6103–6107.
(17) Bohm, H.-J., Schneider, G., Eds. *Protein−Ligand Interactions: From Molecular Recognition to Drug Design*; Wiley-VCH: Weinheim, Germany, 2003; pp 3−20.
(18) Baum, B.; Muley, L.; Smolinski, M.; Heine, A.; Hangauer, D. G.; Klebe, G. Unpublished results.
(19) Humphrey, W.; Dalke, A.; Schulten, K. VMD: visual molecular dynamics. *J. Mol. Graphics* **1996**, *14*, 33–38.
(20) Sturzebecher, J.; Sturzebecher, U.; Vieweg, H.; Wagner, G.; Hauptmann, J.; Markwardt, F. Synthetic inhibitors of bovine factor Xa and thrombin comparison of their anticoagulant efficiency. *Thromb. Res.* **1989**, *54*, 245–252.
(21) Dixon, M. The graphical determination of Km and Ki. *Biochem. J.* **1972**, *129* (1), 197–202.